A new method to detect the vortex glass phase and its evidence in YBCO

2008 J. Phys.: Condens. Matter 20 385211

(http://iopscience.iop.org/0953-8984/20/38/385211)

J. Phys.: Condens. Matter **20** (2008) 385211 (8pp) doi:10.1088/0953-8984/20/38/385211

A new method to detect the vortex glass phase and its evidence in YBCO

M G Adesso[1], **M Polichetti and S Pace**

Physics Department, SUPERMAT, INFM, University of Salerno, Via S Allende, 84081, Baronissi (Salerno), Italy

E-mail: adesso@sa.infn.it

Received 16 May 2008, in final form 6 August 2008
Published 27 August 2008
Online at stacks.iop.org/JPhysCM/20/385211

Abstract

The evidence of the vortex glass phase has been obtained by analysing the nonlinear magnetic response of type-II superconductors. The method introduced here is based on a combined frequency dependence analysis of the real and imaginary part of the 1st and 3rd harmonics of the AC magnetic susceptibility. The analysis has been performed by taking into account both the components and the Cole–Cole plots (i.e. the imaginary part as a function of the real part). Numerical simulations have been used to identify the fingerprints of the magnetic behaviour in the vortex glass phase. These characteristics allowed the vortex glass phase to be distinguished from the other disordered phases, even those showing similar electrical properties. Finally, this method has been successfully applied to detecting the vortex glass phase in an YBCO bulk melt-textured sample.

1. Introduction

Experimental and theoretical studies on the 'effective zero resistance' in the voltage–current characteristics of type-II superconductors, are widely reported in the literature [1]. Huse *et al* [2] argued for the existence of a second order thermodynamic phase transition between a vortex phase, with a small but nonzero resistivity, and a truly superconducting phase, named *vortex glass*, with no mobile vortices and thus strictly zero resistivity. In this latter phase, the vortices were supposed frozen into a configuration determined by the competition between the interactions of the vortices with each other and with the microscopic impurities in the material [2]. The Kim–Anderson model [3] is generally used to describe the vortex dynamics, and in particular the thermal activation processes (flux creep [4]) in the phase with nonzero resistance, whereas several models [5–7], e.g. the vortex glass collective creep models [8], have been developed to explain the resistivity approaching zero, characteristic of the vortex glass phase. These two different approaches are mainly distinguished by the dependence of the pinning potential (U_p) on the current density (J): a linear $U_p(J)$ is supposed in the Kim–Anderson model whereas all the vortex glass models are characterized by a nonlinear $U_p(J)$. Consequently, in the presence of a vortex glass phase, a negative curvature has to be detected in a $\log I$–$\log V$ plot [2], for a temperature T lower than the vortex glass phase transition temperature, T_g, in sharp contrast with the Kim–Anderson Flux Creep prediction, which generates a positive curvature [3, 4].

In the literature there is an open question about the interpretation of the glass like behaviour of the vortex matter. Some experimental evidence can be found about this phase transition. Koch *et al* [9] showed a negative curvature in a temperature range $T < T_g$ in the voltage–current characteristics measured on epitaxial YBCO film samples, which can be interpreted in terms of the vortex glass phase. They also measured the critical exponents which are consistent with those expected for this phase transition [5, 9]. Nevertheless, the interpretation of the Koch experimental data [9] is controversial: Coppersmith *et al* [10] and Landau *et al* [11, 12] showed that the standard Kim–Anderson approach, modified with a inhomogeneous pinning potential, $U_p(x)$, depending on the spatial position x, also reproduced the qualitative features of Koch's V–I characteristics [9], and in particular the negative curvature in the E–J curves at low temperatures, thus leaving still open the real interpretation of Koch's data [12]. In this sense, the voltage–current characteristics are not suitable for clearly identifying the presence of a vortex glass phase.

Here we show an innovative method to identify the vortex glass phase, based on the analysis of the nonlinear magnetic

[1] Author to whom any correspondence should be addressed.

response of the samples, in particular on the frequency dependence of the fundamental and higher harmonics of the AC magnetic susceptibility, at a fixed amplitude of the AC magnetic field. Moreover, comparing numerical results and experimental data, obtained on a YBCO melt-textured sample, we report the detection of the vortex glass phase in the analysed material.

2. Simulations of harmonics of the AC magnetic susceptibility

The 1st and 3rd harmonics of the AC magnetic susceptibility as a function of temperature have been simulated by integrating the one-dimensional nonlinear diffusion equation (x = linear dimension, t = time) for the magnetic field inside the sample (B) [13]:

$$\frac{\partial B}{\partial t} = \frac{\partial}{\partial x}\left[\left(\frac{\rho\,(B,J,T)}{\mu_0}\right)\left(\frac{\partial B}{\partial x}\right)\right] \tag{1}$$

where $\rho(B, J, T)$ is the resistivity associated with the vortex movements. This one-dimensional equation describes the behaviour of an infinite slab well, so it can be used to analyse the magnetic response of a sample which can be approximated by it. An equivalent one-dimensional equation is also used to describe the magnetic response of an infinitely long cylinder.

From equation (1), the field profiles $B(x, t)$ inside the sample have been computed and the spatial mean $\langle B(t)\rangle$ of $B(x, t)$ has been obtained, which represents the magnetic induction field inside the sample. The corresponding magnetization M is computed as follows:

$$M = \langle B(t)\rangle - H_{\text{ext}}, \tag{2}$$

where H_{ext} is the external magnetic field; in this case, in absence of a DC field:

$$H_{\text{ext}} = h_{\text{AC}}\cos(\omega t) = \text{Re}\left\{h_{\text{AC}}\text{e}^{\text{i}\omega t}\right\} \equiv \text{Re}\left\{\tilde{\tilde{H}}\right\}. \tag{3}$$

The magnetization, in terms of the Fourier components, can be written as follows:

$$M(t) = \sum_n M_n\cos(\omega_n + \varphi_n) = \text{Re}\left\{M_n\text{e}^{\text{i}(\omega_n+\varphi_n)}\right\} \equiv \text{Re}\left\{\tilde{\tilde{M}}\right\}. \tag{4}$$

Finally, the complex AC magnetic susceptibility is computed as:

$$\chi_{\text{AC}} = \frac{\tilde{\tilde{M}}}{\tilde{\tilde{H}}}, \tag{5}$$

the 1st and 3rd harmonics corresponding to $n = 1$ and 3 in the Fourier components of the magnetization, respectively. Further details about the numerical computation of the harmonics of the AC magnetic susceptibility starting from (1) are in [13].

Several $\rho(B, J, T)$ dependences on the field (B), temperature (T) and current density (J) have been investigated, corresponding to different V–I characteristics [13–17]. Here we report the simulations obtained by using the formula [5, 18]:

$$\rho(B, J, T) = \rho_{\text{FF}}(B, T)\text{e}^{-\left(\frac{U_{\text{p}}(J,T)}{k_{\text{B}}T}\right)}. \tag{6}$$

In (6) $\rho_{\text{FF}}(B, T)$ is the flux flow resistivity, given by the Bardeen Stephen model [1, 19]:

$$\rho_{\text{FF}}\,(B, T) = \rho_{\text{n}}(T)\frac{B}{H_{\text{c2}}(T)}, \tag{7}$$

where ρ_{n} is resistivity in the normal state (in the present simulation: $\rho_{\text{n}}(T) = 40 + 2.2 \times 10^{-1}[T + 273.16\ \text{K}]$) and $H_{\text{c2}}(T)$ is the temperature dependent upper critical field, chosen as in [13, 20]:

$$H_{\text{c2}}(T) = H_{\text{c2}}(0)\frac{\left[1 - \left(\frac{T}{T_{\text{c}}}\right)^2\right]}{\left[1 + \left(\frac{T}{T_{\text{c}}}\right)^2\right]}, \tag{8}$$

where $H_{\text{c2}}(0) = 112$ T, which is a typical value for YBCO bulk samples [13].

The $U_{\text{p}}(T, J)$ in the equation (6) is the pinning potential [1, 5], which depends on the temperature and the current density (in the absence of the DC field):

$$U_{\text{p}}(T, J) = U_0 f(T)F(J, T). \tag{9}$$

The current density dependence of U_{p} is associated with the vortex dynamics and in particular to the Flux Creep models. In order to probe different flux creep models, previous studies [14–16] have been performed, also based on the analysis of the 1st and 3rd harmonics Cole–Cole plots, but at a fixed frequency and various amplitudes of the AC magnetic field. The previous analysis of the harmonics dependence on the amplitude of the AC magnetic field [14–16], performed by using the same numerical technique as the present work, showed that, in order to reproduce the experimental curves measured on some type-II superconductors, in particular YBCO and MgB_2, a further dependence on h_{AC} had also to be included in the pinning potential: $U_{\text{p}} \propto h_{\text{AC}}^{-\beta}$, through a parameter β [15, 16]. Depending on the β value, a similar general behaviour was detected in the curves simulated with all the considered flux creep models [14–16]. Nevertheless, a preliminary qualitative agreement [16] has been obtained between the experimental data [14, 15] and the numerical curves [16] simulated by including the vortex glass flux creep, at different regimes depending on the material. In the present simulations, this amplitude dependence has not been taken into account, the curves being simulated at a fixed h_{AC} (so that just a constant value should be included).

In the numerical computations, the following density current dependence has been used [8]:

$$F(J, T) = \frac{1}{\mu}\left[\left(\frac{J_{\text{c}}\,(T)}{J}\right)^{\mu} - 1\right], \tag{10}$$

with different μ values: 1/7 for single vortex, 3/2 for small bundle, 7/9 for large bundle vortex glass collective flux

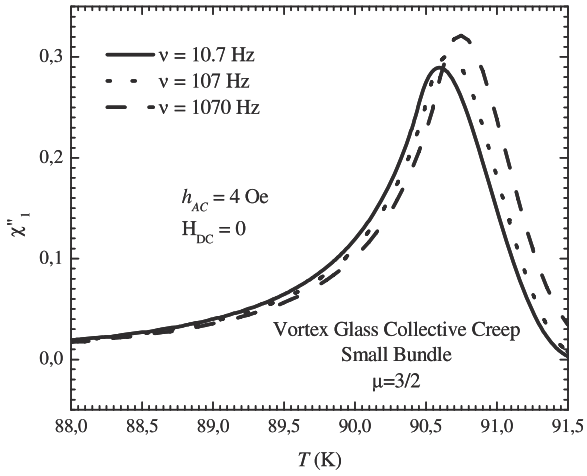

Figure 1. Imaginary part of the 1st harmonics as a function of the temperature as simulated by using the vortex glass collective creep in the small bundle regime, at various frequencies. The curves obtained for the single vortex and large bundle regimes (not reported) show similar qualitative behaviour.

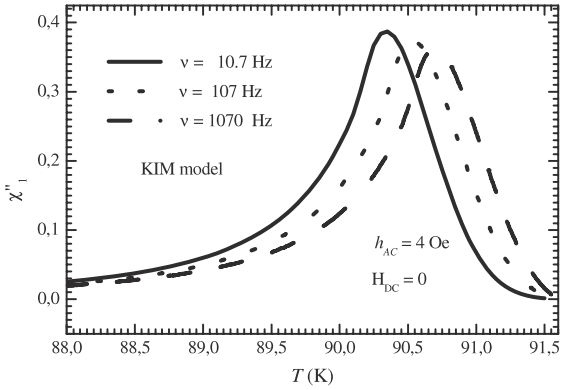

Figure 2. Temperature dependence of the imaginary part of the 1st harmonics at various frequencies, simulated by using the Kim–Anderson model.

creep [8] and −1 corresponding to the linear Kim–Anderson Flux Creep model [3], whereas the phenomenological model [5] $F(J,T) = \ln(\frac{J_c(T)}{J})$, corresponding to $\mu \to 0$ in the (10) has not been considered here. J_c in equation (10) is the critical current density [1, 5].

On the other side, the temperature dependence of U_p and J_c is related to the flux pinning model. The behaviour of the harmonics with different pinning models has been already investigated [13]. Here we only report the results obtained by choosing the δl-type collective pinning [21, 5]. This choice is justified by the previously reported [22] strong evidence for the importance of δl pinning in stoichiometric yttrium-based superconductors. Moreover, an experimental confirmation of the validity of this pinning model was also previously obtained in a polycrystalline YBCO sample obtained from the same batch as the one measured in this work [23]. For these reasons, the following temperature dependences were used in the numerical simulations here shown:

$$U_p(T) \propto \left[1 - \left(\frac{T}{T_c}\right)^4\right] \equiv f(T) \tag{11}$$

$$J_c(T) = J_c(0)\frac{\left[1 - \left(\frac{T}{T_c}\right)^2\right]^{5/2}}{\left[1 + \left(\frac{T}{T_c}\right)^2\right]^{1/2}}. \tag{12}$$

Moreover, U_0 and $J_c(0)$ are the pinning potential and the critical current density at $T = 0$, $H = 0$, $J = 0$, respectively. The values of the parameters used in the simulations are: $T_c = 91.6$ K, $J_c(0) = 10^9$ A/(m^2), and $U_0/k_B = 1.6 \times 10^4$ K. These parameters have been experimentally obtained on the sample analysed in the present work. In particular, T_c and $J_c(0)$ have been measured by magnetization curves, whereas U_0/k_B has been obtained by a combined analysis of the 1st and 3rd harmonics of the AC magnetic susceptibility [24].

We performed simulations at a fixed amplitude of the AC magnetic field ($h_{AC} = 4$ Oe), without a DC field, at various AC frequencies ($\nu = 10.7$, 107, 1070 Hz), by choosing the above mentioned different Flux Creep models.

3. Numerical results

In this section, we summarize the comparison between all the numerically obtained results, in order to identify the fingerprints of the vortex glass phase.

3.1. The vortex glass models versus the homogeneous Kim–Anderson case

A preliminary analysis based on numerical simulation has been previously performed [25]. Here we also report the main results obtained, in order to clearly identify the characteristics of the vortex glass phase with respect to the other disordered phases. In figure 1, the temperature dependence of the imaginary part of the 1st harmonics, at various frequencies of the AC magnetic field, is shown, as simulated in the vortex glass collective creep model, in the small bundle regime. Similar results have been also obtained for single vortex [25] and large bundle regimes (not reported). The same conditions are used to simulate the 1st harmonics in the framework of the Kim–Anderson model, as reported in figure 2.

From figure 1, we can observe that, in the vortex glass phase, for increasing frequencies, the temperature of the peak in the imaginary part of the 1st harmonics, T_p, shifts towards higher temperatures and the height of the peak, $\chi''_1(T_p)$, grows. Nevertheless, in the Kim–Anderson model (figure 2), T_p also shifts towards higher temperatures if ν is increased, but $\chi''_1(T_p)$ decreases.

On the contrary, no qualitative differences can be observed in the behaviour of the real part of the 1st harmonics at various frequencies, in both models [25]. The opposite behaviour with the frequency in the Kim–Anderson Creep and the vortex glass models can be also detected if we analyse the 1st harmonics Cole–Cole plots, as shown in figure 3.

In fact, the height of the maximum in the 1st harmonics Cole–Cole plots decreases for increasing frequencies in

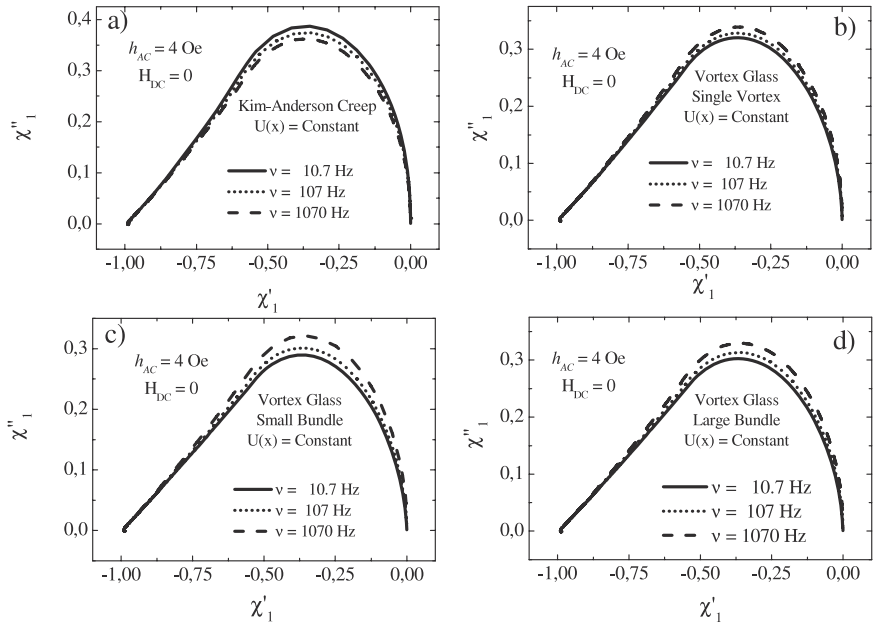

Figure 3. 1st harmonics Cole–Cole plots at various frequencies, simulated by using the Kim–Anderson model (a) and vortex glass collective creep model, respectively, in the single vortex (b), small bundle (c) and large bundle regime (d).

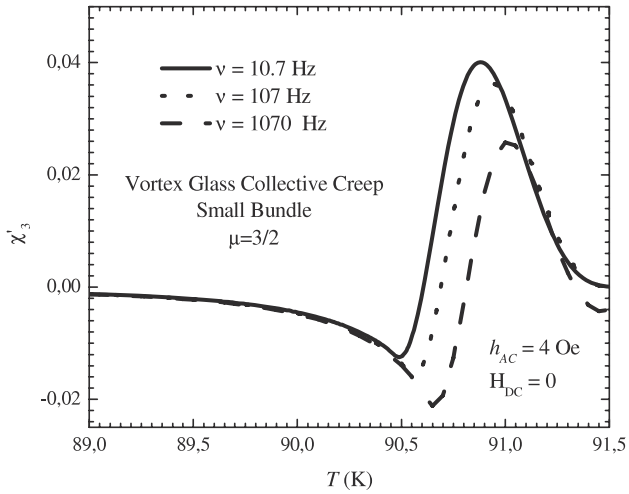

Figure 4. Temperature dependence of the real part of the 3rd harmonics at various frequencies, as simulated with the vortex glass collective creep model in the small bundle regime.

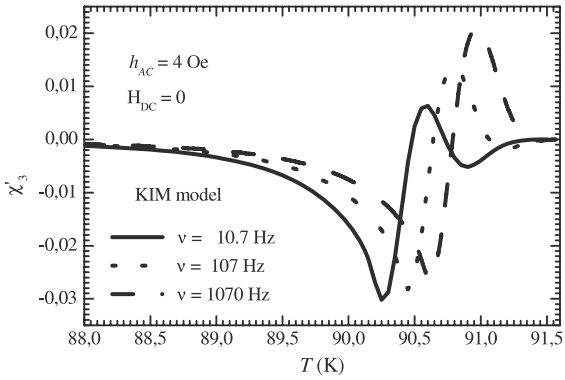

Figure 5. Temperature dependence of the real part of the 3rd harmonics at various frequencies, as obtained by using the Kim–Anderson model.

the Kim–Anderson model, whereas an opposite behaviour characterizes the vortex glass models, in all regimes.

A similar analysis can be also performed on the higher harmonics of the AC magnetic susceptibility. The main differences between the vortex glass and the 'resistive' phase can be seen if we observe the real part, $\chi_3'(T)$, of the 3rd harmonics, whereas a similar behaviour has been detected in the imaginary part of the 3rd harmonics [25].

In figure 4, the real part of the 3rd harmonics of the AC susceptibility simulated in the vortex glass phase (in the small bundle regime) are shown, at various frequencies. In figure 5 the corresponding curves, as obtained by using the Kim–Anderson model, are reported.

From figures 4 and 5, we observe that, in all the considered models, $\chi_3'(T)$ shows a minimum and a maximum, both depending on the frequency. Nevertheless, for increasing frequencies, in the glass phase the absolute value of the minimum grows and the maximum decreases, whereas the behaviour is opposite in the Kim–Anderson framework.

A more distinct frequency response can be seen in the 3rd harmonics Cole–Cole plots, reported in figure 6 for all the considered models.

From figure 6 we observe that the 3rd harmonics Cole–Cole plots point towards the right semi-plane progressively for increasing frequencies in the Kim–Anderson model, whereas they tend to the left semi-plane in the vortex glass phase, for all the regimes.

In conclusion, we can state that the frequency dependence of the imaginary part of the 1st harmonics and the real part of the 3rd harmonics, together with both the 1st and 3rd

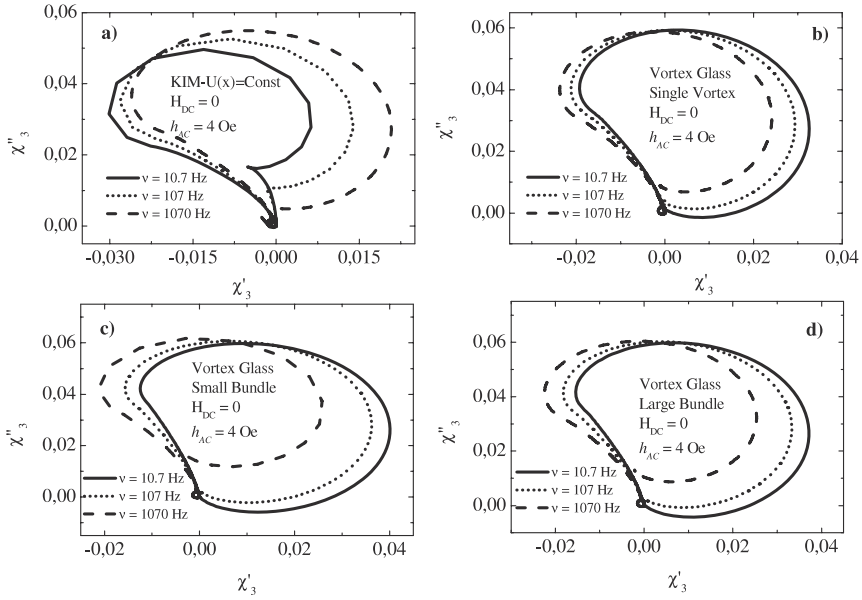

Figure 6. 3rd harmonics Cole–Cole plots at various frequencies, simulated by using (a) the Kim–Anderson model and (b)–(d) the vortex glass collective creep model, respectively in the single vortex (b), small bundle (c) and large bundle (d) regime.

harmonics Cole–Cole plots, without a DC field, allow one to distinguish a vortex glass phase from the phase described by the Kim–Anderson model.

3.2. A comparison between the vortex glass and the inhomogeneous Kim–Anderson case

In the literature [11, 12], the standard Kim–Anderson approach, modified with an inhomogeneous pinning potential, $U(x)$, is supposed to be equivalent to the vortex glass collective creep, because it reproduces some qualitative features of the voltage–current characteristics, associated with the occurrence of a vortex glass phase [2].

The choice of the $U(x)$ dependence does not influence the main features of the analysis [12] but, in order to reproduce the Koch [9] V–I characteristics, it is also necessary to include a further temperature dependence, strictly connected to the x-dependence [12]. According to [12], we chose the following model for $U(x, T)$:

$$U(x,T) \propto \left(|x| - a\left[1 - \left(\frac{T}{T_c}\right)\right]^k x^2 \right) \equiv h(x,T) \qquad (13)$$

where $x = 0$ corresponds to the semi-thickness of the sample.

The parameters used in our simulations are: $a = 1$ and $k = 1.5$ [12].

In figure 7 the imaginary part of the 1st harmonics and the real part of the 3rd harmonics as a function of the temperature are reported at various frequencies, as simulated with this inhomogeneous pinning model within the Kim–Anderson framework. The corresponding 1st and 3rd harmonics Cole–Cole plots are plotted in figure 8.

It is possible to see that the imaginary part of the 1st harmonics is characterized by a positive peak shifting towards higher temperatures with a decreasing height, for increasing

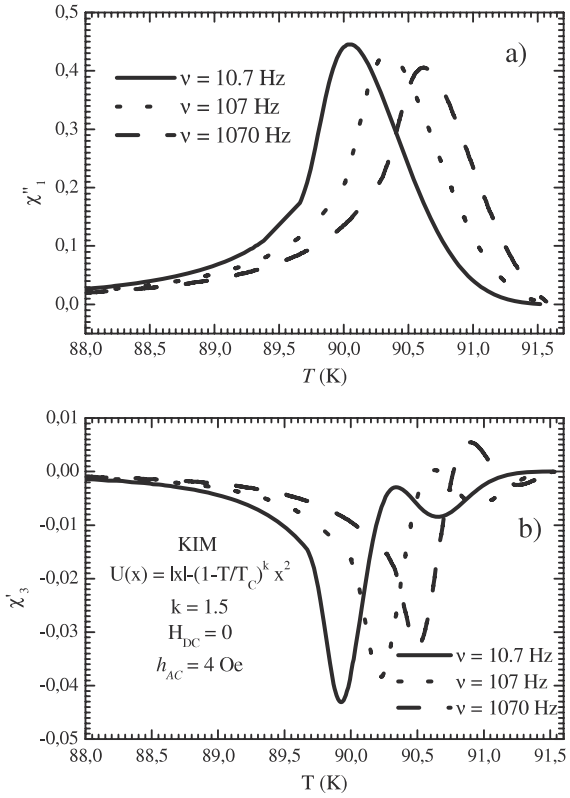

Figure 7. Imaginary part of the 1st harmonics (a) and real part of the 3rd harmonics (b) as a function of the temperature, simulated by using an inhomogeneous Kim–Anderson model at various frequencies.

frequencies. Moreover, two peaks can be distinguished in the real part of the 3rd harmonics: for increasing frequencies the height of the positive peak near T_c increases, whereas the

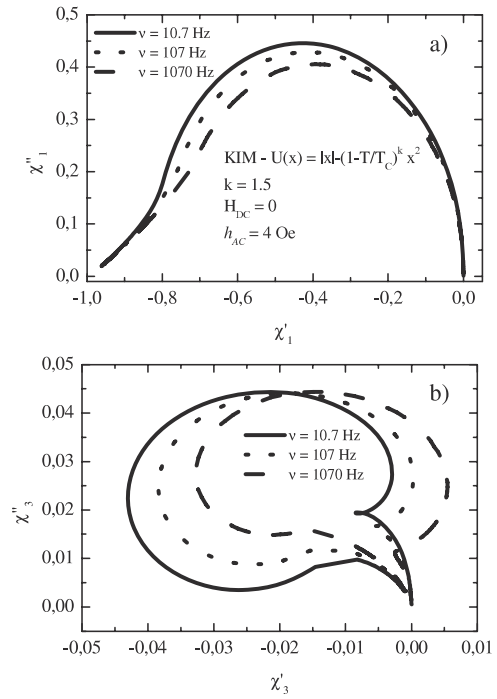

Figure 8. 1st (a) and 3rd (b) harmonics Cole–Cole plots at various frequencies, computed by using an inhomogeneous Kim–Anderson model.

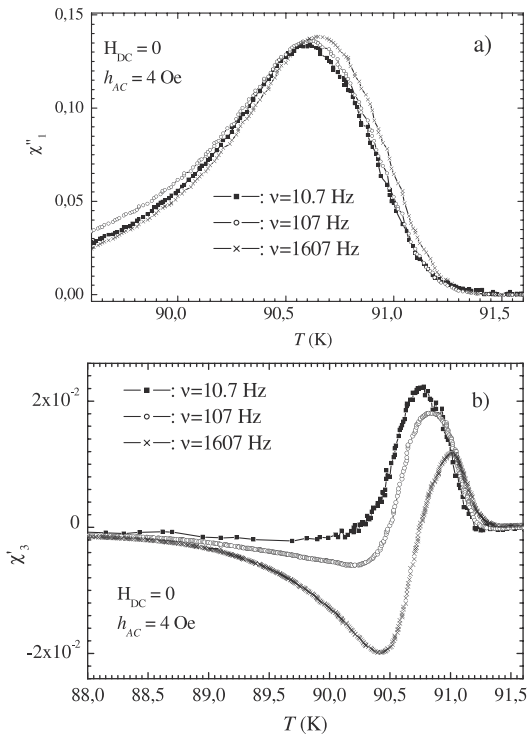

Figure 9. Imaginary part of the 1st harmonics (a) and real part of the 3rd harmonics (b) as a function of the temperature, as measured on an YBCO sample at various frequencies and at a fixed amplitude of the AC magnetic field.

height of the negative peak at lower temperatures decreases in absolute value. The 1st harmonics Cole–Cole plots are characterized by a maximum which decreases for increasing frequencies, whereas the 3rd harmonics Cole–Cole plots tend to the right semi-plane for higher frequencies. All these dependences are similar to the results obtained with the standard Kim–Anderson model, and are opposite to the curves simulated with the Vortex Glass models.

Therefore, from this analysis, it is possible to conclude that the vortex glass phase has a different behaviour with respect to a phase described by the Kim–Anderson Flux Creep model, both in the homogeneous and inhomogeneous case.

4. A method to detect the vortex glass phase

Summarizing the previous results, a good method to identify a vortex glass phase is to analyse the behaviour of the harmonics of the AC magnetic susceptibility by changing the frequency of the AC magnetic field, without a DC field. In particular, a vortex glass phase can be detected if, for increasing frequencies:

(1) in the imaginary part of the 1st harmonics versus T, the height of the peak increases;
(2) in the real part of the 3rd harmonics versus T, the absolute value of the minimum at low temperatures grows and the height of the maximum near T_c decreases;
(3) in the 1st harmonics Cole–Cole plots, the height of the maximum increases;
(4) the 3rd harmonics Cole–Cole plots point towards the left semi-plane.

The harmonics described by the Kim–Anderson model have an opposite behaviour in all these cases. This analysis furnishes a method to experimentally detect a vortex glass phase by magnetic measurements, thus overcoming the problem connected to the 'real zero resistivity' in the direct transport measurements.

5. Experimental evidence of the vortex glass phase

The above introduced method is quite general and it could be applied to any type-II superconductors. Here we used it to analyse the experimental results obtained on an YBCO bulk melt-textured sample. The measured sample was a melt grown YBCO sample, cut as an almost homogeneous slab (2 mm × 3.1 mm × 4.8 mm), obtained from the same batch previously analysed [26]. An home made susceptometer was used to measure the 1st and 3rd harmonics of the AC magnetic susceptibility as a function of the temperature at various frequencies (ν = 10.7, 107, 1607 Hz) and amplitudes (h_{AC}) of the AC magnetic field, both with and without an external DC field (H_{DC}). The harmonics have been measured by applying both the AC and the DC magnetic fields parallel to the longitudinal axis of the sample.

In figure 9, the imaginary part of the 1st harmonics and the real part of the 3rd harmonics are plotted at various frequencies as a function of the temperature. In figure 10, the 1st and 3rd harmonics Cole–Cole plots are shown, as measured at the same conditions. In figure 11, the imaginary part of the 1st harmonics and the 1st harmonics Cole–Cole plots are shown,

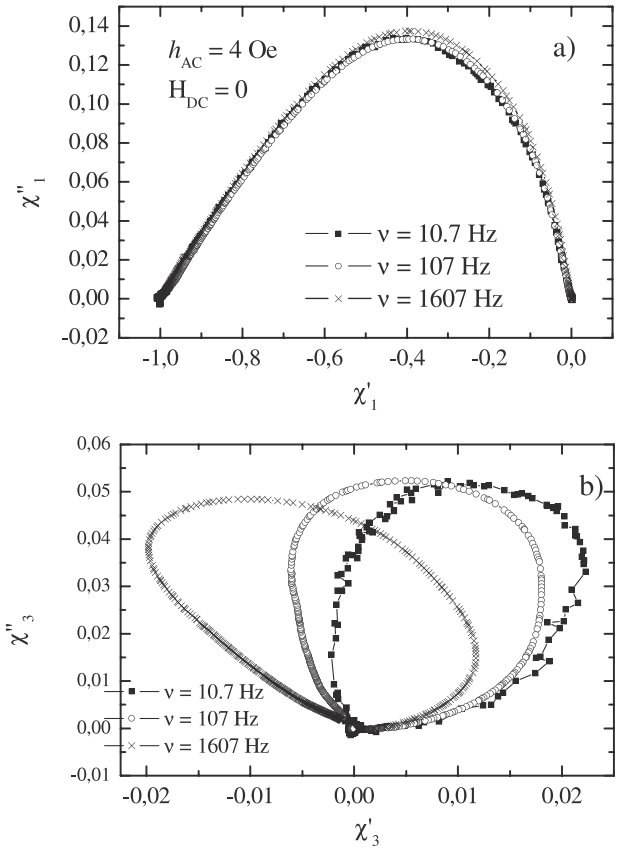

Figure 10. 1st (a) and 3rd (b) harmonics Cole–Cole plots, as measured on the YBCO sample at various frequencies.

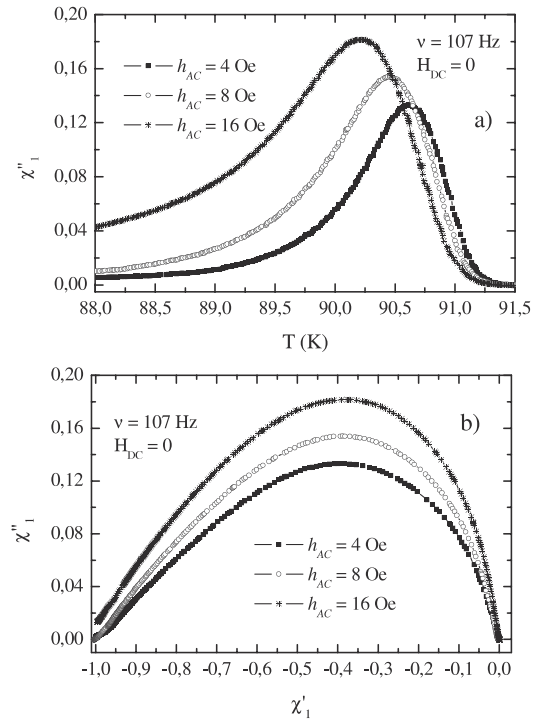

Figure 11. Imaginary part of the 1st harmonics (a) and 1st harmonics Cole–Cole plots (b) measured on YBCO melt-textured at various amplitudes of the AC magnetic field, without a DC field.

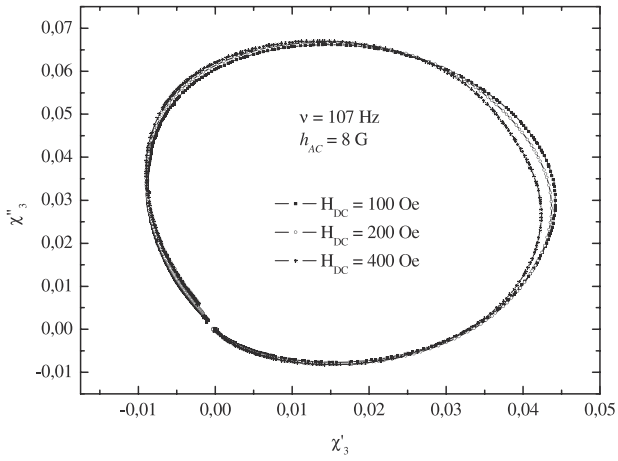

Figure 12. 3rd harmonics Cole–Cole plots, measured at a fixed frequency and amplitude of the AC magnetic field, at various DC fields, measured on the same YBCO sample: the half cardioid/lent shaped curves are in agreement with the simulations [31] obtained by including the bulk screening.

as measured at various amplitudes of the AC field, at a fixed frequency and without a DC field.

The data reported in figures 9–11 suggest that the effects due to an eventual granularity, which could exist in our sample [27, 28], are not present. In fact, as it is known [1, 29, 30], in the case of a granular sample, the AC magnetic response is characterized by two contributions, i.e. the inter-grain and the intra-grain components. These can be seen as a double peak in the imaginary part of the 1st harmonics versus temperature curves (as well as a corresponding double-step transition in $\chi'_1(T)$), and as two joined dome shaped curves in the 1st harmonics Cole–Cole plots. From figures 9–11, we deduced that the effects of granularity can be neglected, even if external parameters like the amplitude and the frequency of the AC magnetic fields are changed. The absence of the granularity has also been confirmed through measurements in the presence of different DC fields (not shown here).

From figures 9 and 10 we observe that all the characteristics of the vortex glass phase, described in the previous section, have been detected. In particular, in the 3rd harmonics for increasing frequencies the absolute value of the minimum at low temperatures grows, the maximum near T_c decreases, and the Cole–Cole plots tend toward the left semi-plane. Moreover, the presence of the vortex glass phase is also confirmed by a slightly, but still evident, growth of the maximum in $\chi'_1(T)$ and of the maximum in the 1st harmonics Cole–Cole plots with the frequency.

It is worth underlining that this behaviour in the 3rd harmonics Cole–Cole plots could also be interpreted in terms of a edge barrier. In order to exclude this possibility, we also performed some measurements of harmonics at various DC fields. In figure 12 the 3rd harmonics Cole–Cole plots are reported, at various DC fields up to 400 Oe, as measured at a fixed AC field. The comparison between these curves and the simulations reported in [31] suggest that the surface effects can be disregarded. In fact, our curves have a lent/half

cardioid shape, lie in a single quadrant, and behave almost independently of the applied DC field. All these characteristics are common to the curves simulated in [31] in the case of a bulk pinning, and are totally different from those simulated in presence of edge effects that are cardioid in both the semi-planes.

On the basis of this analysis and by using the method introduced in section 4, we finally conclude that the data reported here in figures 9 and 10 are experimental evidence of the occurrence of a vortex glass phase in a YBCO melt-textured sample, with negligible granularity and surface effects.

6. Conclusions

We introduced an effective method to identify the vortex glass phase in a type-II superconductor, based on the nonlinear magnetic response of the samples. In order to develop this method, numerical simulations of the harmonics of the AC magnetic susceptibility have been performed, at various frequencies of the AC magnetic field, by using different flux creep and flux pinning models. In particular, we demonstrated that the frequency dependence in the magnetic response simulated by using the Kim–Anderson flux creep model (both considering the homogeneous and the inhomogeneous flux pinning model) is different from the magnetic behaviour in the vortex glass phase. Moreover, thanks to a comparison between numerical results and experimental data, the vortex glass phase has been successfully detected in an YBCO bulk sample.

References

[1] Tinkham M 1996 *Introduction to Superconductivity* 2nd edn (New York: McGraw-Hill)
[2] Huse D A, Fisher M P A and Fisher D S 1992 *Nature* **258** 553
[3] Hempstead C F and Kim Y B 1964 *Phys. Rev. Lett.* **12** 145
[4] Anderson P W 1962 *Phys. Rev. Lett.* **9** 309
[5] Blatter G, Geshkenbein V B and Larkin A I 1994 *Rev. Mod. Phys.* **66** 1125
[6] Fisher M P A 1989 *Phys. Rev. Lett.* **62** 1415
[7] Feigel'man M V, Geshkenbein V B, Larkin A I and Vinokur V M 1989 *Phys. Rev. Lett.* **63** 2303
[8] Wen H H, Hoekstra A F TH, Griessen R, Yan S L, Fang L and Si M S 1997 *Phys. Rev. Lett.* **79** 1559
[9] Koch R H, Foglietti V, Gallagher W J, Koren G, Gupta A and Fisher M P A 1989 *Phys. Rev. Lett.* **63** 1511
[10] Coppersmith S N, Inui M and Littlewood P B 1990 *Phys. Rev. Lett.* **64** 2585
[11] Landau I L and Ott H R 2000 *Physica* C **340** 251
[12] Landau I L and Ott H R 2002 *Phys. Rev.* B **65** 64511
[13] Di Gioacchino D, Celani F, Tripodi P, Testa A M and Pace S 1999 *Phys. Rev.* B **59** 11539
[14] Adesso M G, Polichetti M and Pace S 2004 *Physica* C **401/1-4** 196
[15] Adesso M G, Senatore C, Polichetti M and Pace S 2004 *Physica* C **404/1-4** 289
[16] Adesso M G, Polichetti M, Senatore C and Pace S 2003 Cole–Cole plots of the 1st and the 3rd harmonics of the AC susceptibility for the study of dissipative phenomena in type II superconductors *Proc. to the EUCAS* pp 2117–24 (Settembre 2003, Sorrento)
[17] Senatore C, Polichetti M, Zola D, Di Matteo T, Giunchi G and Pace S 2003 *Sup. Sci. Technol.* **16** 183
[18] Ling X and Budnick J I 1991 AC susceptibility of type II superconductors: vortex dynamics *Magnetic Susceptibility of Superconductors and Other Spin System* ed R A Hein *et al* (New York: Plenum) pp 377–88
[19] Bardeen J and Stephen M 1964 *Phys. Rev.* **136** A1485
[20] Coffey M W and Clem J R 1992 *Phys. Rev.* B **45** 9872
[21] Larkin A I and Ovchinnikov Yu N 1979 *J. Low Temp. Phys.* **34** 409
[22] Polichetti M, Pace S and Vecchione A 1999 *Int. J. Mod. Phys.* B **13** 1101
[23] Griessen R, van Dalen A J J, Dam B, Rector J and Schnack H G 1994 *Phys. Rev. Lett.* **72** 1910
[24] Polichetti M, Adesso M G and Pace S 2003 *Eur. Phys. J.* B **36** 26
[25] Polichetti M, Adesso M G and Pace S 2004 *Physica* A **339/1-2** 119
[26] Boffa M, Di Trolio A, Pace S, Saggese A, Vecchione A, Camarota B and Sparvieri N 1997 *IEEE Trans. Appl. Supercond.* **7** 1797
[27] Li S, Fistul M, Deak J, Metcalf P, Giuliani G F, McElfresh M and Kaiser D L 1995 *Phys. Rev.* B **52** R739
[28] Lewis J A, Vinokur V M, Wagner J and Hnks D 1995 *Phys. Rev.* B **52** R3852
[29] Ozogul O 2005 *Phys. Status Solidi* a **202** 1793
[30] Polichetti M, Gömöry F and Pace S 1998 *Phys. Lett.* A **249** 140
[31] van der Beek C J, Indenbom M V, D'Anna G and Benoit W 1996 *Physica* C **258** 105